2021•2022

Faculteit Industriële Ingenieurswetenschappen

master in de industriële wetenschappen: elektronica-ICT

Masterthesis

Feasibility of artificial synapses using thin film photovoltaic materials and architectures

PROMOTOR :

Prof. dr. Bart VERMANG

PROMOTOR :

prof. dr. Zacharie JEHL LI-KAO

Pieter Paulissen

Scriptie ingediend tot het behalen van de graad van master in de industriële wetenschappen: elektronica-ICT

Gezamenlijke opleiding UHasselt en KU Leuven

2021•2022

Faculteit Industriële Ingenieurswetenschappen

master in de industriële wetenschappen: elektronica-ICT

Masterthesis

Feasibility of artificial synapses using thin film photovoltaic materials and architectures

PROMOTOR :

Prof. dr. Bart VERMANG

PROMOTOR :

prof. dr. Zacharie JEHL LI-KAO

Pieter Paulissen

Scriptie ingediend tot het behalen van de graad van master in de industriële wetenschappen: elektronica-ICT

UHASSELT

KU LEUVEN

Foreword

I am proud to present you my master's thesis on feasibility of artificial synapses using thin film photovoltaic materials and architectures. Due to the fact that solar cells have become an important feature in daily life, I thought it is very interesting to anticipate the topic in a research group where they are conducting investigation regarding thin film solar cells. I knew my topic would not be the development of thin-film solar cells, but it is a beginning of research on the memory effect of thin film solar cells.

I started my study as an industrial engineer in 2017 at the university of Hasselt in Belgium. After the first semester, I was convinced about which specialization to choose. I was most interested in programming and electronics. Once I was in my specialization, I immediately noticed that I had chosen the right field.

I was convinced from the very first moment to do my internship at the research center of the Polytechnic University of Catalonia (UPC) at The Photovoltaic Group. This internship gave me the opportunity to work on the aforementioned topic conducting research and tests. I got the opportunity to help my colleagues, by writing an analysis tool in the way they desired. Furthermore, I had the opportunity to learn more about topics I never deepened in my study program.

I want to thank several people who helped and taught me a lot during my internship, but also who made my experience more enjoyable. I would like to thank Prof. Dr. Zacharie Jehl and Axel Gon Medaille for supporting and helping me every day and for the help they provided me with my master thesis. I also want to thank Dr. Kunal Tiwari and Dr. Marcel Placidi for helping me during my internship. In addition, I would like to thank Prof. Dr. Bart Vermang, my supervisor from Belgium, for making this internship possible together with Karin Evers and for their unconditional support. Finally, I would also like to thank my other colleagues for helping me and providing me an unforgettable Erasmus.

Thank you for your time and consideration. I wish you a pleasant reading.

Table of Contents

List of Tables

List of Figures

Wordlist

AL	Artificial intelligence
ALU	Arithmetic logic unit
ANN	Artificial neural network
CIGS	Copper-indium-gallium-selenide solar cell
CPU	Central processing unit
CZTS	Copper-zinc-tin-sulfide solar cell
DSSC	Dye sensitized solar cell
E_g	Band gap energy
IR	Infrared
I_{SC}	Short circuit photocurrent
LTD	Long term synaptic depression
LTP	Long term synaptic potentiation
MLP	Multilayer perceptron
MPP	Maximum produced power
PPF	Paired-pulse facilitation
SCPI	Standard commands for programmable instruments
SLP	Single layer perceptron
STP	Short term plasticity
V_{OC}	Open circuit voltage

Abstract (English)

The Photovoltaic Group, at the Polytechnic University of Catalonia does research on inorganic thin film solar cells in parallel with the research on the memory effect of inorganic thin film devices. This solar cell is supposed to be the basic block of an artificial neural network which aims to address the limitations the von Neumann architecture, namely its high energy consumption, by unifying the computing and memory units.

A new electrical analysis tool was developed in Python. Using this analysis tool and an LED-based solar simulator, the memory effect of an inorganic thin film solar cell, CIGS (Copper-indium-gallium-selenide solar cell), can be studied. By modifying the wavelengths, the illumination time, and altering the bias voltage, long term plasticity (LTP) can be detected and characterized.

Changing the wavelengths has shown that only a limited number of wavelengths is usable for creating an analog memory. Using infrared light makes it possible to probe the state of a device, that is whether the synapse is charge (potentiated) or discharged (depressed). An Analog memory effect can be obtained both in the dark at a bias voltage higher than 0 V and under light illumination in short-circuit current condition. Inorganic thin film solar cells show memory effect, but to finely tune the output value of the solar cell, more research is needed. Research on material characterization and the influence of the wavelength, the illumination time, and the bias voltage would be pertinent in the near future.

Abstract (Dutch)

De fotovoltaïsche groep, aan de Polytechnic University of Catalonia doet onderzoek naar anorganische dunne-film zonnecellen, parallel met het onderzoek naar het geheugeneffect van anorganische dunnefilmzonnecellen. Deze zonnecel wordt verondersteld de basisblok te zijn van een artificial neuraal netwerk dat de beperkingen van de von Neumann-architectuur, namelijk het hoge energieverbruik, wil aanpakken door de reken- en geheugeneenheden te verenigen.

Een nieuw elektrisch analyse-instrument werd ontwikkeld in Python. Met behulp van dit analyse-tool en een LED zonnesimulator kan het geheugeneffect van een anorganische dunne-film zonnecel, CIGS (koper-indium-gallium-selenide zonnecel), worden bestudeerd. Door de golflengten, de bestralingstijd en de biasspanning te wijzigen, kan long term plasticiteit gedetecteerd en gekarakteriseerd worden.

Het veranderen van de golflengten heeft aangetoond dat slechts een beperkt aantal golflengten bruikbaar is voor het creëren van een analoog geheugen. Het gebruik van infrarood licht maakt het mogelijk de toestand van een apparaat te peilen, d.w.z. of de synaps is opgeladen of ontladen. Een analoog geheugeneffect kan worden verkregen zowel in het donker als bij verlichting met licht. Anorganische dunne-film zonnecellen vertonen een geheugeneffect, maar om de uitgangswaarde van de zonnecel nauwkeurig af te stellen is meer onderzoek nodig. Onderzoek naar materiaalkarakterisering en de invloed van de golflengte, de bestralingstijd, en de biasspanning zou in de nabije toekomst relevant zijn.

1. Introduction

1.1 Basic of machine learning

1.1.1 Introduction

Machine learning is something humans encounter every day, usually even without knowing it.. Social media, smartphones, hospitals are all examples where machine learning is used every day. It is already crucial now and it will only become quasi ubiquitous in the future. Through machine learning, humans are able to process large amounts of data in a faster way instead of doing it themselves. In addition, daily processes can be automated and optimized. Allowing you to make better decisions. With the help of machine learning, growth is and can be accelerated and improved in all facets[1].

1.1.2 Principle of the learning process in a human brain

The pattern formation of neuronal activities leads to the modification of specific synaptic connections. The brain's ability to learn and memory effect is the result of these neuronal activities. A pre-neuron is connected to a post neuron through a synapses, when the pre neuron fires, the signal is transmitted with a specific weight which depends on the potentiation of the synapse. The strengthening and weakening of synapses, referred to as plasticity, is an important feature here. This plasticity can be long lasting (several seconds up to several years) as in long term synaptic potentiation (LTP) or depression (LTD). LTP occurs with high frequency stimulation, while LTD occurs with low frequency stimulation. This can for example be illustrated with reference[2], where LTP can dominate LTD in a time window of 70 ms. In this process, LTP tends to override LTD, but LTD is able to cancel LTP[2].

Short term plasticity (STP) is a behavior of some milliseconds or less, where the system quickly returns to its initial state. Another form of short term plasticity is paired-pulse facilitation (PPF), also known as activity dependent synaptic plasticity[3].

Neurons receive stimuli and are interconnected through synapses thanks to which they can exchange information. These stimuli are electrical impulses and each impulse has a different strength. The stimulus comes from the presynaptic neuron and goes to the postsynaptic neuron via the synapse[4]. The efficiency of the synapse to transmit a stimulus is determined by its synaptic plasticity (weight). The efficiency of the signal can be excitatory or inhibitory. If a previous neuron has an excitatory effect on the current neuron, the probability that the current neuron will take a 'fire action' will increase. While with an inhibitory effect, this probability will decrease. The neuron will integrate all received signals. When the result of the integration is greater than a defined threshold, the neuron will 'fire'. This will create an electrical signal to all the other connected neurons. Figure 1 shows the working of a biological principle of a neuron.

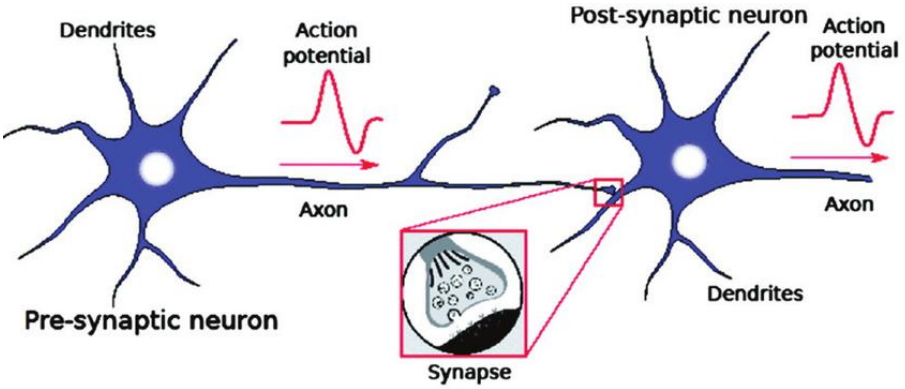

Figure 1: Biological principle of a neuron[5]

1.1.3 Perceptron: as basic neural network

Artificial intelligence (AI), deep learning, artificial neural networks (ANN) are terms which lead us to believe smart computers were only developed in recent years. Contrarily to popular belief, the origin of a neural network lies in the 1950s. Frank Rosenblatt designed the first neural network, called the perceptron[6]. He was inspired by the functioning of the human brain, more specifically the biological principle of a neuron.

Frank Rosenblatt's perceptron consists of a neuron receiving different input signals, it is the simplest form of an ANN. Each input signal is multiplied by a weight vector. Then, all those signals will be summed together. When the result of the sum is larger than a certain threshold, the neuron will emit a signal. So in the case of the perceptron, a "1" will be sent at the output. When the sum is smaller than the certain threshold, a 0 will be sent at the output.

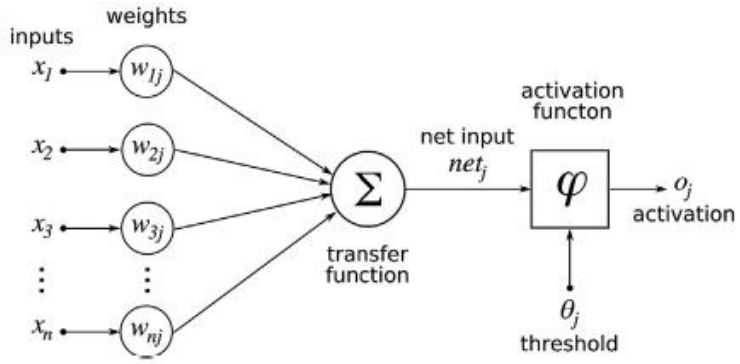

Figure 2: Frank Rosenblatt's perceptron model[7]

Pattern detection is a machine learning algorithm who is able to automatically recognize patterns and regularities in data. Images, text and sounds are all examples of the data. This system can recognize familiar patterns very accurate and very quickly.

1.1.4 Differences between supervised and unsupervised learning

A supervised learning algorithm uses labeled data, which means that labels must be created before the data can be used to train the model. Furthermore, features must also be created to train the model in a better way. To create a good data set, the action of a person is always needed before the model can be trained. Usually a supervised neural network uses backpropagation. The working principle of backpropagation is as follows: first the obtained output is compared with the required output. Based on this result, an error is calculated. This error is then used to fine tune the weights of the neural

network using backpropagation[7]. The goal for supervised learning is to predict the outcomes of new data, such as: spam detection, price predictions, weather forecasting.

The main difference between a supervised and an unsupervised learning algorithm is the data set. An unsupervised learning algorithm uses an unlabeled data set and no features need to be created. By training the model properly and obtaining good weights, the model should be able to detect different features based on the weights in hidden layer(s)[8]. Regarding on methods of fine tuning the weights in supervised learning, it is clear that this is done based on the final result (the error). However, neurons in our brains fine tune "the weights" (synapses) locally and not based on the final result. This is clearly shown in “winner takes it all” networks. Here, one neuron in the layer will become active (win) and all the other neurons remain inactive. So only the active neuron will respond to this particular input pattern, and only this neuron will have to learn. All the weights that are connected to this learning neuron will be fine-tuned. Since only these weights are fine-tuned and based on one neuron and not the final result, we can conclude that the learning process takes place locally[9]. From this we can see that that the synapses plasticity rule takes place locally. The main goal of unsupervised learning is to get insights from big data sets, to discover hidden and interesting things from data[10].

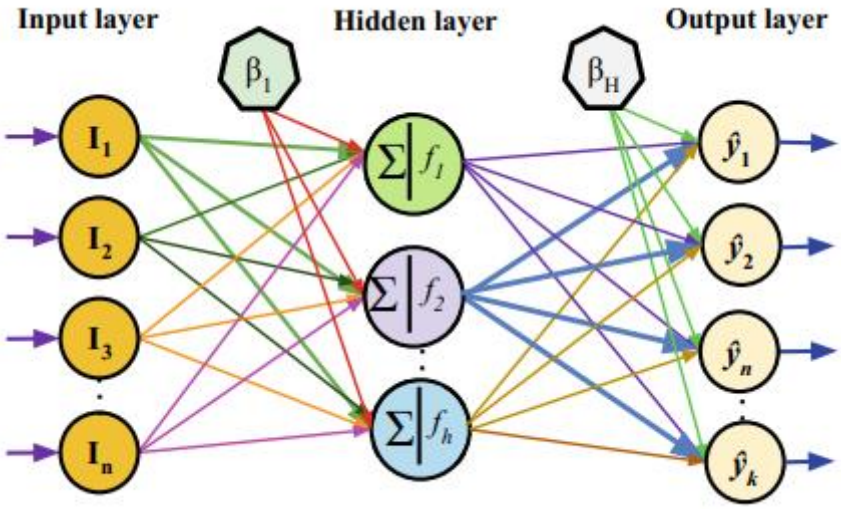

Figure 3: Neural network with 1 hidden layer

Rosenblatt developed a supervised learning algorithm to train the perceptron. The training process is as follows: First, we need to collect data that will allow us to train the model. Next, the data must be labeled so that the training model knows what the outcome must be. Then, features are created and used as input signals. Finally, the data set is divided into 2, the training set and the cross-validation set. The training set is used to train the model. When the model is trained, the cross-validation set is used to check the performance of the trained model. In the training process, the values of the 'weights' of the input signals will always be changed. These determine the result of the sum and also the binary result.

As mentioned previously, the cross-validation set is used to check the performance of the model. To check the model, we use the following methods: accuracy, precision (Positive prediction value), recall and F1 score. The performance of the model cannot be determined with accuracy only. If only 1% of the training data set is labeled with a 0, you can very easily obtain an accuracy of 99% just by giving all test labels a 1.

The precision (1) can be described as, how much of the identified positive was correct. The recall (2) is also known as the sensitivity. The F1 score (3) is one of the possibilities to indicate how good the machine learning model is. The goal is to reach a result equal to 1 for the precision, recall and F1 score. The following equation can be used to calculate these parameters:

1. $precision = \frac{True\ positive}{True\ positive+False\ positive}$,
2. $recall = \frac{True\ positive}{True\ positive+False\ negative}$,
3. $F1 - score = \frac{2\ x\ precision\ x\ recal}{precision+recall}$.

As mentioned earlier, the perceptron is the simplest form of an ANN. It has been shown that the single layer perceptron (SLP) is unable to efficiently detect nonlinear separable patterns. To solve this problem, a multilayer perceptron (MLP) was created. The MLP has at least one hidden layer as shown in Figure 3, but often multiple hidden layers. High learning potential, robustness to noise, nonlinearity, parallelism, fault tolerance and high capabilities in generalizing tasks are the main advantages of the MLP[9]. The MLP can be trained by using supervised learning and unsupervised learning.

As mentioned earlier, a neuron receives a stimulus that is able to transmit information through a synapse. In unsupervised learning according to Hebbian theory the information is passed on in the same way and consequently learned in the same way. Hebbian learning is based only on activities and not on error signals or labels[11].

1.1.5 The limitations of existing architectures

Typically, algorithms above are running on computers with the von Neumann architecture, as shown in Figure 4. The stored program concept is used here: the central processing unit (CPU) and the memory unit are separated from each other and communicate using a shared bus. The CPU consists of an arithmetic logic unit (ALU) and a control unit which is referred as the computational part. Between the CPU and the memory unit significant amount data is transported, consequently a considerable amount of energy is used[12]. Currently, the von Neumann architecture is mainly used to execute the learning algorithm. As mentioned earlier, numerous calculations are needed when training a learning algorithm. Because of this, there will be constant back and forth communication between the CPU and memory unit, here we encounter the bottleneck of the von Neumann architecture. Because of these communications, a significant amount of energy is used and a certain amount of time is required before the model is trained. Also the computing process takes some energy and time, but the energy and time from the data exchange between the CPU and memory is significantly higher.

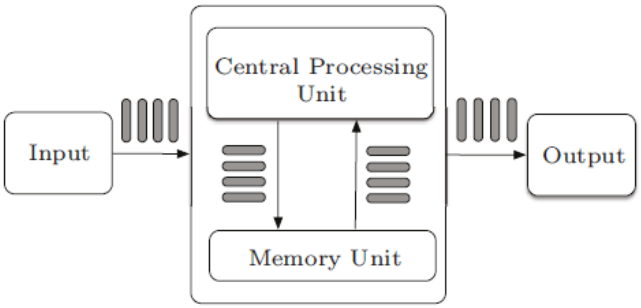

Figure 4: von Neumann architecture[13]

To use an unsupervised machine learning algorithm in a faster and more energy efficient way, a solution must be found for the bottleneck in the von Neumann architecture or another technology/architecture must be created. With the von Neumann architecture, the solution must be found in the software by changing the algorithm in an efficient way, because the hardware is fixed. Another solution is to create a new network based only on hardware components and not using digital capabilities. In this analog network we will try to recreate basic brain function (building blocks) using highly stable inorganic materials. These buildings blocks will be called artificial synapses. Because 80% of the brain gets his info from light, solar cells and photosensors with memory capability are an interesting research pathway in that regard.

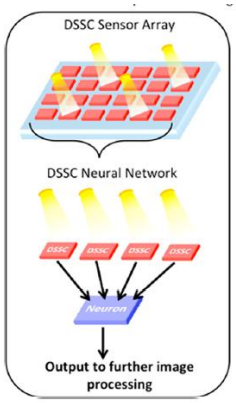

Figure 5: ANN using solar cells[14]

In this research, thin film solar cells with intrinsic defects existing either in the bulk of a special layer, or at the interface between two layers, will be used. The following section will provide additional insights on the mechanisms possibly leading to a synaptic behavior.

1.2 Solar cells

1.2.1 Basic of the p-n junction

Optoelectronic artificial synapses can use the photovoltaic effect, which is the generation of electron-hole pairs by light illumination and the subsequent electromotive force induced by their selective extraction. So it is necessary to understand how a solar cell works. Typically, solar cells are a junction between two semiconductors of different doping that is p and n. In a p-type (respectively n-type) semiconductor, the number of holes (resp electrons) is greater and they ensure the electrical current. Connecting the p and n semiconductor creates a depletion region devoid of carriers (p-n junction) and the induced electric field (built in potential) allows to selectively transport only one type of carrier in one direction. Thus, a p-n junction can be viewed as a double selective contact for carriers, and thus behaves like a diode. For the sake of simplicity, we can assume that both the p and n material have a similar bandgap and only differ in their doping nature.

When the solar cell is exposed to light, a photon will penetrate the surface. When the energy of the photon is lower than the bandgap energy (E_g), the photon is not absorbed and it is transmitted through the film. A photon with an energy value greater than E_g will create an electron-hole pair at the output[15]. Solar cells can typically be characterized using an I-V analysis under illumination or in the dark, that is measuring the output current for different values of an applied voltage, Figure 6 shows the I-V characteristic of a solar cell in the dark and under illumination. When the I-V characteristic of a solar cell is measured in the dark, the "dark curve" is obtained, typical of a diode. Here the curve will cross the axes at the origin. The I-V characteristic under illumination will shift to the curve downward as a result of the photogenerated charge carriers. Hereby a short circuit current and an open circuit

voltage will be created. At a specific point, the power produced will be maximum (MPP), which is used to calculate the conversion efficiency of the cell $\frac{P_{out}}{P_{in}}$. The bottom right corner of the dark rectangle is the maximum power output of the solar cell. It should be highlighted that the photocurrent is a minority carriers current (electrons in the p-region, holes in the n-region).

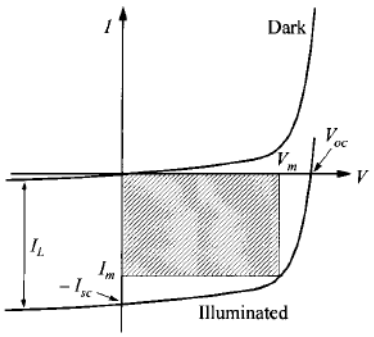

Figure 6: I-V characteristic of a solar cell in the dark and under illumination[15]

Figure 7 shows the energy band diagram of a solar cell. As shown in the Figure 7, the energy band diagram is composed of holes in the valence band and electrons in the conduction band. Between these, as mentioned earlier, is the forbidden energy band gap corresponding to E_g. In the following, we assume for simplicity reason that the light absorption only occurs in the p-type material, though the principle would be unchanged and symmetrical if considering absorption in the n-type material. The energy of a photon enables an electron to move from the valence band to the conduction band, while a hole is created in the valence band. This phenomenon is called electron-hole pair generation, though the holes can be ignored at the first order as the hole population in a p-type material is large enough to screen the photo-hole generation in the considered conditions. In this process, the number of electrons in the conduction band will increase, these electrons are also called the minority-carriers. The separation between holes and electrons creates an internal voltage in the material. Photogenerated electrons are able to diffuse towards the space charge region where they can be selectively transferred to the n-type material, the shape of the electric field in the space charge region prevents them to diffuse back to the p-type material; hence, an electronic current (photocurrent) appears. The situation is symmetrical for the holes, and the movement of the holes is opposite to the movement of the electrons, thus creating the current. The main limitation of this mechanism is the undesirable effect of non-radiative recombination. In this process, minority carriers leave the conduction band and return to the valence band. Because of recombination, the number of minority-carriers will reduce and as a result, the current/voltage will reduce.

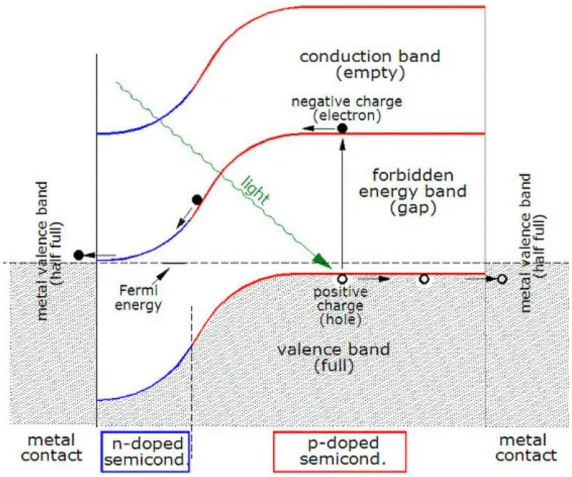

Figure 7: Energy band diagram[16]

1.2.2 Defects and electron traps

The Fermi energy is the statistical position of charge carriers in the material, following the Fermi-Dirac statistic (which can be approximated to the Boltzmann statistic at room temperature). It can be viewed as the surface of the sea of electrons at 0 K. In an equilibrium situation, the position of the Fermi level depends on the type of the dominant carriers; generally, for the materials considered, the Fermi level is close to the valence band in p-type materials, and close to the conduction band in n-type materials. When holes and electrons are separated, each population can be defined with its own Fermi level: we then talk about quasi-Fermi levels, and their energetic separation is the internal voltage resulting from illumination. Impurities, imperfections in the crystal, mismatch at the p-n interfaces etc. can create additional energy levels within the bandgap. These levels, referred to as defects, can trap charge carriers ("traps") and favor electron hole recombination ("recombination centers"). In some cases, the trapping of electrons in a defect will significantly modify the carrier transport properties (photoconductivity) of the material even for a long time after the illumination has ceased. This "persistent photoconductivity" can be seen as a memory effect of the cell, which "remembers" the past illumination stimulus. Such mechanism can be used to create a mimicry of brain synapse and simulate similar plasticity functions.

1.3 Artificial synapses

1.3.1 Basic principles

When light illuminates the solar cell, a current will flow as mentioned earlier. Electrons will move from the conduction band to the valence band, and will then flow from the p region to the n region. As shown in Figure 8, there can also be one or more extra energy levels (defects) inducing a metastability state to the system. Depending on the characteristics of this level, an electron can remain trapped for several milliseconds up to several hours. This will affect the properties of the material while electrons occupy this intermediate state, and such behavior is known within the photovoltaic community as "light soaking" of a solar cell. The fact that such an electron can (temporarily) get trapped in an energy level ensures that we can use the solar cell as a memory cell[17], if we are able to properly identify the figure of merit to be used as an output to the system.

Following an illumination (stimulus), we thus characterize the solar cell in the dark and the identification of a persistent photoconductivity (for example, higher current after illumination at a given voltage) resulting from trapped electrons is a marker of the synaptic plasticity of the system. The timeframe during which electrons remain trapped determine the nature of the plasticity.

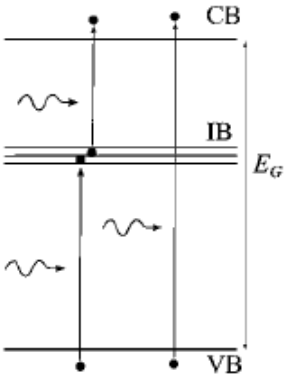

Figure 8: Energy band diagram with an intermediate band (IB)[17]

1.3.2 Example: artificial synapses using DSSC

A first way to test the electrical plasticity of solar cells is by continuous light illumination. In this configuration, stimulation and output collection happen simultaneously, and the system is self-powered from the stimulation itself. The electrical plasticity is examined on the basis of duration of light illumination. The figure of merit chosen as output is the short-circuit photocurrent (I_{SC}), which changes a function of the stimulation duration. Electrical plasticity has been studied with such approach using dye sensitized solar cells (DSSCs)[14]. To determine the change of J_{SC} (ΔJ_{SC}), first a measurement is done without light illumination. Then 5 other measurements with light illumination were made in a time range from 5 minutes to 40 minutes. ΔJ_{SC} in relation to time is shown in Figure 9. Here it is clearly visible that ΔJ_{SC} continues increasing during the first 20 minutes. After this period, almost no changes are visible. We can conclude that light sources with shorter exposure than 20 minutes are less important for DSSCs. The exposure from 20 minutes can be called important optical input.

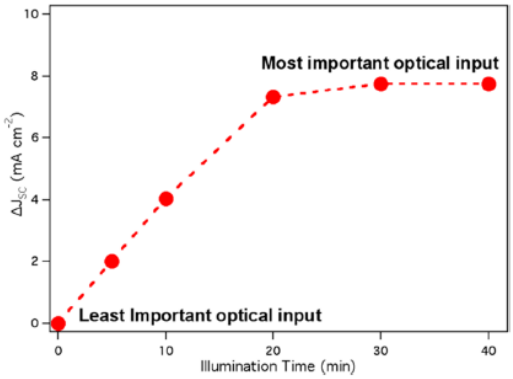

Figure 9: ΔJ_{SC} during continues light illumination at 100 mW/cm²[14]

Next, the time-dependent learning of lighting was investigated. First, J_{SC} was determined before illumination. After this, the solar cell was illumination for 5 min and then placed again in the dark at open circuit. From then on, several measurements were performed by which the learning rate of the DSSC can be determined. The result of these measurements are shown in Figure 10a. After 5 minutes of light illumination we notice that J_{SC} has decreased by about 2 mA/cm², this is also visible in Figure 9. After 10 minutes in the dark we clearly see a memory loss, resulting in almost returning to its original equilibrium state. Next, these measurements are repeated, but this time with an illumination time of 40 minutes. Also after this illumination duration we immediately do a measurement and we observe

that J_{SC} has decreased by about 8 mA/cm², as shown in Figure 10b and Figure 9 again. In this measurement, it is clearly visible that in the beginning J_{SC} increases quickly, but after 5 minutes this increasement of J_{SC} starts to slow down, and then stabilizes after about 20 minutes. Here we do see a clear difference between the new state and the original state[14]. Figure 10b clearly shows that LTP occurs. To make a correct conclusion about Figure 10a more tests have to be done just after the light illumination. When the J_{SC} value returns to its (quasi) original state within a few milliseconds we are talking about STP otherwise the conclusion can be made that LTP also occurs here, but that the effect is not as long present as with light illumination of 40 minutes.

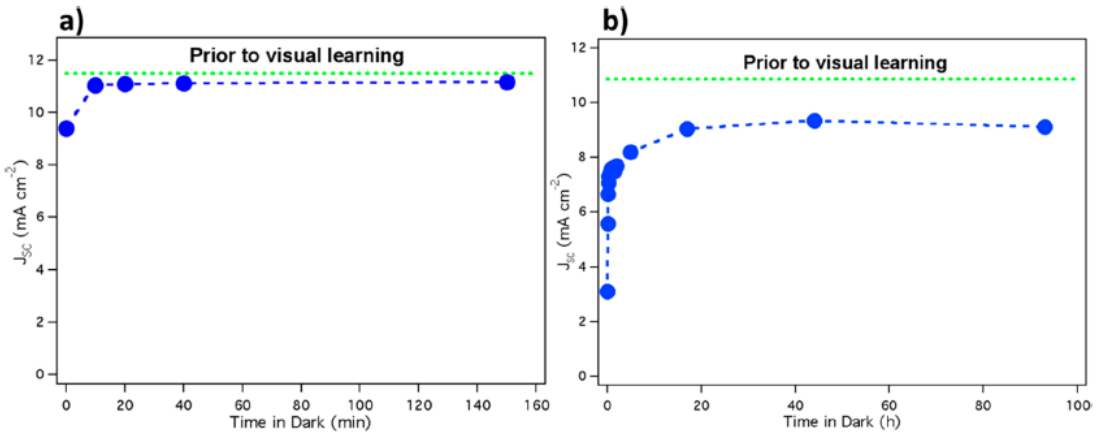

Figure 10: a) J_{SC} resting in the dark after a continues illumination for 5 minutes (at 100 mW/cm²) - b) J_{SC} resting in the dark after a continues illumination for 40 minutes (at 100 mW/cm²)[14]

Another research that also important is to investigate, is the possibility to obtain a deep learning process from certain optical inputs. We can (possibly) obtain this by having the solar cell learn repeatedly. Through cycles of light illumination followed by resting in the dark. In an earlier study it was chosen to use a light illumination of 20 minutes each time followed by a resting period of 17 hours[14]. Figure 11 shows the result after 6 repetitions. Then, comparison can be made with the result from Figure 10b. Here it is visible that the value of J_{SC} after about 95 hours in the dark is 9 mA/cm². When a learning process with repeated light illuminations takes place we see that after six cycles the value of J_{SC} has dropped to 7 mA/cm². The conclusion is that deep learning has occurred.

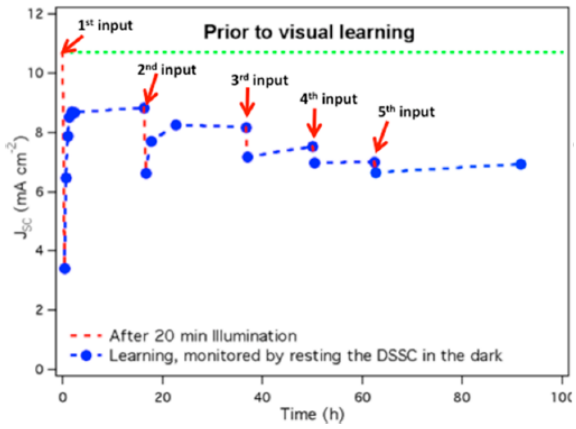

Figure 11: Cycles of light illumination (20 minutes) followed by resting in the dark (17 hours)[14]

1.3.3 Conclusion

A similar research study as with the DSSC can also be done with inorganic materials that have previously demonstrated other forms of metastabilities. The materials considered are, the p-doped is

CuZnSnSe2 (CZTS) and the n-doped is a CdS buffer layer, completed by an intrinsic ZnO layer which oxygen content can be varied. In addition to investigating the STP and LTP as a consequence of illumination duration and cycles of illumination time, the influence of different wavelengths will be investigated. These are important parameters as objective is to reproduce basic human brain functions. Where 80% of the information is received through light. Furthermore, it should also be clarified that an optoelectronic artificial synapse is a sensor and has its own memory, thus avoiding the bottleneck of the von Neumann architecture.

2. Methods and materials

The methods and materials section will be longer and more detailed than usual as a new characterization tool has been developed in the course of this project. This section will explain why it was important to develop a new characterization tool and how it works. After, it will explain which samples, materials and methods are used during testing.

2.1 Characterization tool

To analyze the behavior of a synapse, we need a tool that is time-dependent, fast, and can measure at a specific voltage. This is not possible with the existing analysis tools in PV laboratories, which focus on analyzing the figures of merit of a classic solar cell device. Hence, a new tool had to be developed that is able to perform these measurements specific to synaptic plasticity. To do these measurements, the Keithley model 6430 sub-Femtoamp remote source meter is used, shown in Figure 12a. The source meter is connected to a computer utilizing Windows OS using a General purpose interface bus (GPIB) cable. The characterization tool is written in Python using PyCharm. The Python library Tkinter has been used to develop the graphical interface Figure 12b.

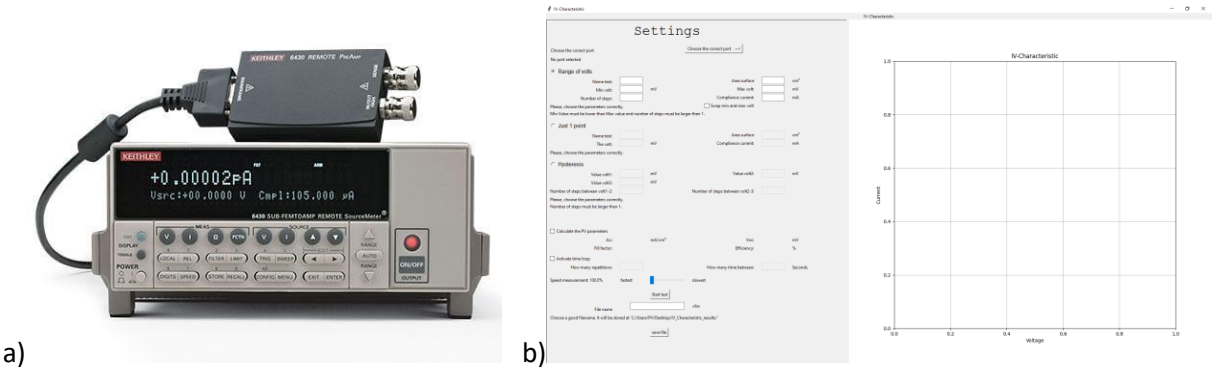

a) b)

Figure 12: a) Keithley mode 6430 sub-Femtoamp remote source meter[18] b) Graphical interface characterization tool

On request of colleagues, the characterization tool has been developed not only for testing synapses, but also to be versatile and for characterizing solar cells. As a result, there are three different test possibilities:

- range of bias – Create an IV-curve, used for standard solar cells,
- just 1 point – Measurement at one specific voltage, which is instrumental when estimating persistent photoconductivity,
- hysteresis,
- All measurements can be preformed as a function of time.

2.1.1 Connection

To set up the connection between the Keithley source meter and the computer, a GPIB connector is used as mentioned earlier. Using the Python library PyVISA, the connection at software level is made. As visible on Figure 13, the 'GPIB::0::INSTR' must be chosen to connect to the source meter. After this, the testing can start.

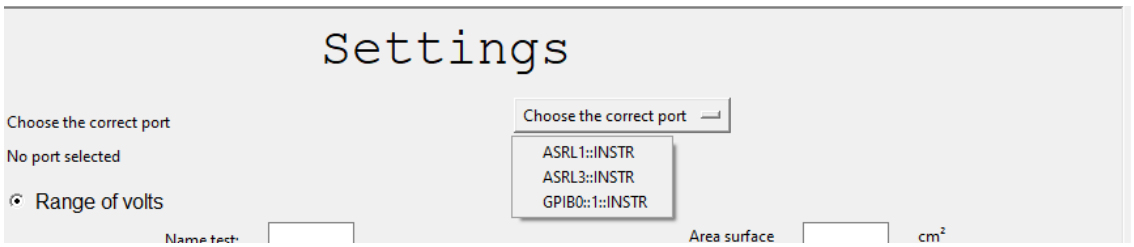

Figure 13: Choose GPIB to connect to the source meter

2.1.2 Range of volts – Create an IV-curve

To create the IV curve, some important parameters beside the name of the test are needed:

- start Voltage (min volt),
- end voltage (max volt),
- number of steps,
- surface area of the cell,
- maximum current (Compliance current).

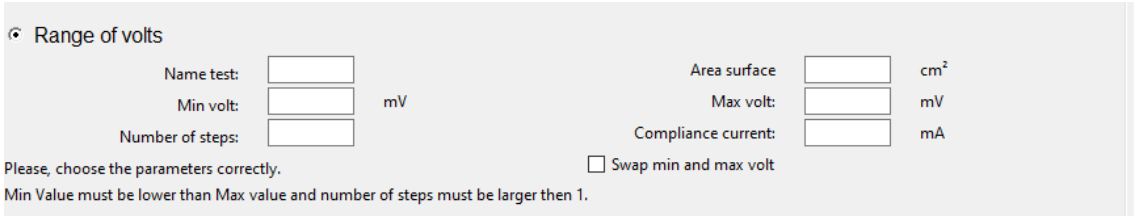

Figure 14: Parameters needed for IV-curve

There is also the possibility to start the test at the highest voltage and thus evolve to the lowest voltage. This can be made possible by checking 'Swap min and max volt'. The test is performed by sending Standard Commands for Programmable Instruments (SCPI) commands to the source meter. Using SCPI commands, the initial voltage and the final voltage together with step size are sent to the source meter. The maximum current is also set in this way.

Before starting the test, there are a few more possible options, as visible in Figure 15:

- calculate the PV-Parameters:
  - short circuit current,
  - open circuit voltage,
  - fill factor,
  - efficiency,
- activate time loop,
- speed of the measurement.

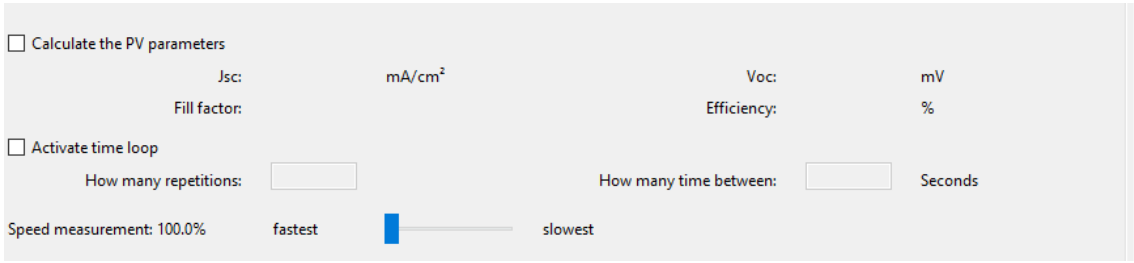

Figure 15: Extra test options IV-curve

When activating the time loop, two parameters need to be filled in. The duration between every measurement in seconds and how many times the measurement need to be repeated. This option can be used, but is not required when measuring an IV curve. *This is in contrast to the speed at which measurements are made.* When the test takes place at maximum speed (100%) with the parameters according to Table 1, the IV curve in Figure 16a is obtained. The measurement took place in 0.8 seconds, but some incorrect points are also visible to local capacitors being created in the device when the voltage variation is too fast for the response time of the solar cell. Then the measurement is performed again with the same parameters but at a speed at 75%. The result of this measurement is visible in Figure 16b. The measurement took place in 0.2 seconds. When reducing the speed, the incorrect data points disappeared, but the test took 5 seconds longer. This is not a problem since 5 seconds on 100 data points is almost insignificant, especially when compared to the test speed of the other analysis tools present in the laboratory.

Table 1: Settings speed test IV-curve

Min. volt (mV)	Max. volt (mV)	Number of steps (/)	Surface area (cm²)	Compliance current (mA)
-100	700	100	0.087	100

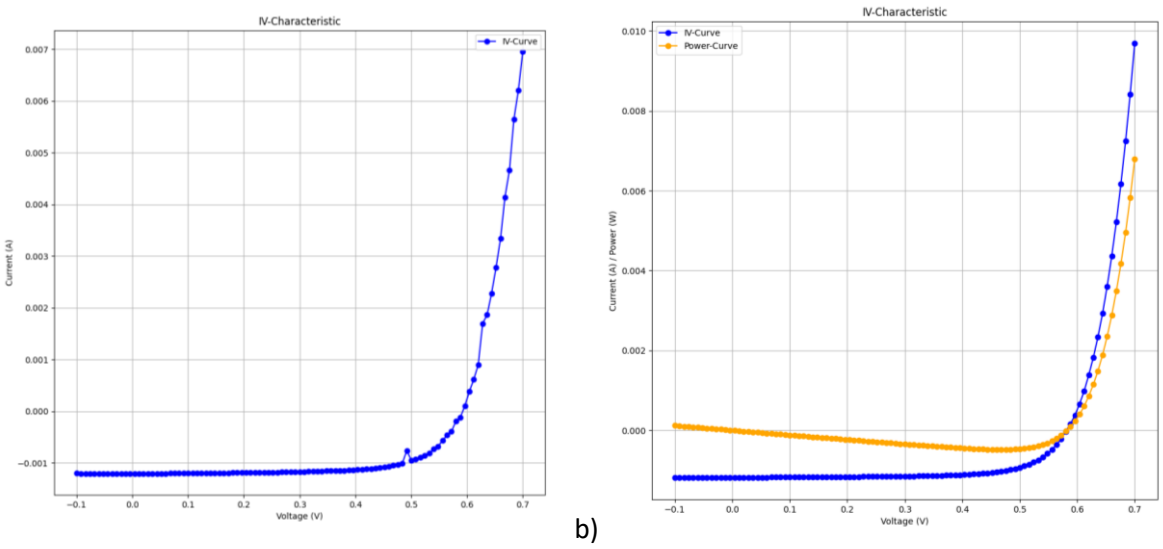

a) b)

Figure 16: a) IV-curve at maximum speed without the calculations of the pv-parameters b) IV-curve at 75% of the maximum speed with the calculations of the pv-parameters

Figure 16a shows the IV curve without calculating the pv-parameters, while Figure 16b shows the IV curve with calculating the pv-parameters. Based on the short circuit current (I_{sc}), the open circuit voltage (V_{OC}) and the power curve, the fill factor (1) and efficiency (2) can be calculated. Using the I_{SC}, the J_{SC} is determined. These are printed as shown in Figure 17. The following two equations are used to calculate the fill factor and the efficiency:

1. $fill\ factor = \frac{P_{Max\ power}}{V_{OC}\ x\ I_{SC}}$,
2. $efficiency = \frac{V_{OC}\ x\ I_{SC}\ x\ Fill\ factor}{P_{in}}$.

Figure 17: Result of calculating the pv-parameters

2.1.3 Just 1 point – Measurement at 1 specific voltage

To create a point measurement, some important parameters beside the name of the test are needed:

- specific Voltage (the volt),
- surface area of the cell,
- maximum current (Compliance current).

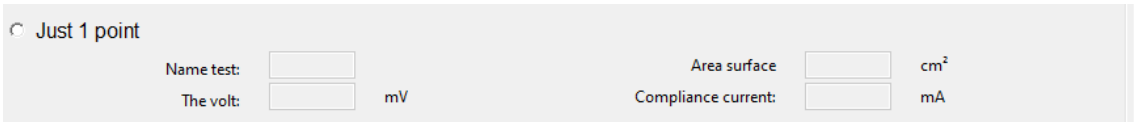

Figure 18: Parameters needed for the point measurement

In addition, here SCPI commands are sent for setting the voltage and the maximum current. Only the time loop activation can be used here as an additional option, this is by far the most important option of observing synaptic behavior. With this option we are able to observe both STP and LTP. To observe LTP we need to measure over a longer period, which is perfectly possible with this option. So for LTP, there are no limitations, this in contrast to STP. For STP, a lot of data must be collected in a short time (a few milliseconds). Tests have shown that the smallest time difference between 2 data points is equal to 0.035 seconds. This is the limitation for measuring STP.

2.1.4 Hysteresis

There are also several important parameters for measuring a hysteresis:

- start voltage (Value volt1),
- intermediate voltage (Value volt2),
- end voltage (Value volt3),
- number of steps between the start and intermediate voltage,
- number of steps between the intermediate and end voltage.

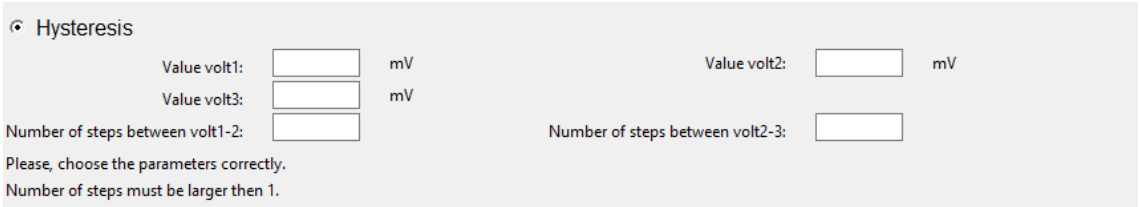

Figure 19: Parameters needed for hysteresis

There is no SCPI command that changes the voltage first with a positive delta V and then with a negative delta V. As a result, all intermediate voltages are calculated in the program and then put into a list. Next, this list is sent to the source meter with an SPCI command, which makes it possible to measure a hysteresis. The inconvenient of this method is that the list cannot exceed 100 values.

2.1.5 Save measurements

It is not necessary to save the data after every measurement, several measurements can be done without saving. When all the desired measurements are finished, the data must be saved. As visible in Figure 20, the following message appears before saving the data: 'Data is not saved'. To save the data, it is required to give a file name and then all the data is saved in an excel file. After this the message disappears.

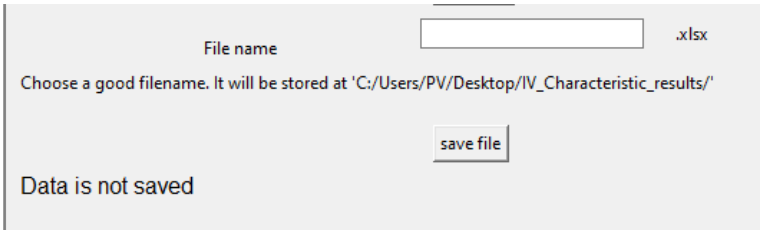

Figure 20: Save the measured data

2.2 Setup

The LED-based G2V solar simulator is used for irradiating the samples. The light emitted by the G2V solar simulator can be adjusted to the desired conditions for the test. 31 different wavelengths from 361nm to 1556nm are available and the intensity of these wavelengths are also tunable. Finally, the distance between the cell and the lens of the G2V solar simulator is also an important factor. To simulate real conditions for solar cells on Earth, the distance between the cell and the lens should be 3 cm, though this parameter is not as critical for a synapse as the goal is not to generate power. Figure 21 shows the setup without a black box.

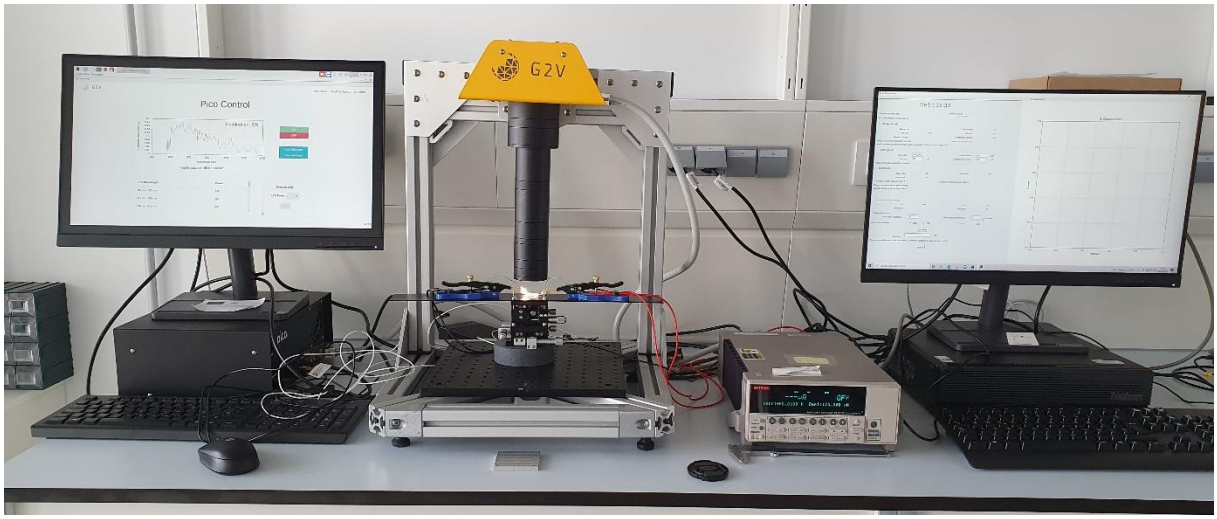

Figure 21: Setup without the black box

2.2.1 The black box

To analyze the memory effect of solar cells, two situations are possible:

- the solar cell under light illumination using the G2V solar simulator;
- the solar cell completely in the dark.

To create these two situations the use of a black box is necessary, as seen in Figure 22. The blue curve is the first "dark" measurement at 700 mV in daylight and without a black box. 17.5 hours later, the test was done again at 700 mV in daylight and without a black box. This resulted in a constant current of 1.2 mA. As a result of this result, it was assumed that 1.2 mA is the value of current for this

discharged cell at 700 mV. Next, the test was performed again under the same conditions. But this time we also tested during the night (in the dark) resulting in the green curve. It is clearly visible that daylight has a great influence on the results. The value of the current at night is equal to 0.5 mA, while it increased to 1.1 mA because of the daylight, these results show that the use of a black box is necessary to obtain correct and reliable results.

The black box will be created in a way where the lens of the solar simulator is present inside the box. This means that during the testing of a particular cell there never will be any change of the setup. Only when changing the test cell, the black box will be removed.

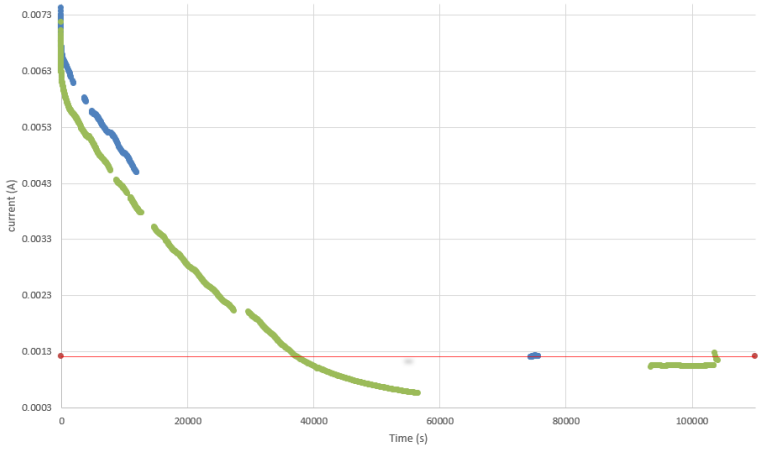

Figure 22: (Blue) First test 'dark' test at 700 mV without black box - (Red) Assumed level of a discharged solar cell by day, without black box – (Green) Dark test at 700 mV during day and night

Creating a black box with appropriate contacting as described earlier requires a period of time. But due to the limited time of my internship, it is impossible to create this black box and collect enough results. As a result, we chose to create a black box using aluminum foil.

2.3 Samples

Since the research center does research on inorganic thin film solar cells, the research on optoelectronic artificial synapses will also use inorganic thin film solar cells. two different solar cells were investigated. The first solar cells are Copper-indium-gallium-selenide solar cell (CIGS) with an i-ZnO layer having an oxygen content of 0%, 5%, 10% or 15%. The other solar cell is recently developed and is a copper-zinc-tin-sulfide solar cell (CZTS).

2.4 Test methods

2.4.1 Long term plasticity

As mentioned earlier, LTP is the occurrence of a memory effect for seconds to several hours. This has been investigated in three different ways. The first way is to expose the cell to light for a certain time and then place it in the dark. The persistent photoconductivity is investigated as a function of time. Thereby, it is investigated what influence the illumination time has on the discharge (shape of the curve and the discharge time).

The influence of different wavelengths on a charged cell is the next research pathway. Every wavelength will be activated separately with a intensity of 1,4 mW/cm². The measurement will start and every 10 seconds the light source will be turned on or off. This will be done at a bias voltage of 0 mV (I_{SC}) and a bias voltage higher than 0 mV.

The last testing pathway is investigating the device in open circuit conditions (I_{sc}), where the influence of light illumination time is investigated, to try reproducing a behavior similar to that of the DSSC reported in reference[14].

2.4.2 Short term plasticity

With the current setup it is impossible to do research to STP. As mentioned earlier, speed of the measurement is limited. It is necessary to have measurements every millisecond to detect STP, while with the current setup, the maximum achieved speed is a measurement every 35 milliseconds. Also PPF is impossible to investigate with the current setup. The solar simulator does not have a function were the light source can be turned on and off at a high speed. An optical chopper need to be added to the setup to investigate PPF and simulated fast light pulses.

3. Results

3.1 The influence of light illumination time

To investigate the process of discharging, the solar cell is first exposed to white sunlight with an intensity of 86.6 mW/cm² for a certain time. Next, the cells are placed in the dark and the current is measured every five minutes at a bias voltage of 700mV. This process is shown in Figure 23 for oxygen (5%-O) CIGS cells. This process shows that hours to days are needed to discharge a solar cell. The red curve is the discharge process after 15 minutes of light illumination. The blue curve is the discharge process after 90 minutes of light illumination. The first major difference is the current just after removing the light source. The current is double after 15 minutes of light illumination compared to the current after 90 minutes of light illumination, which shows a learning behavior of the device. Furthermore, there is also a significant difference in the shape of the curve and consequently in the discharge time. For the red curve, after 20 hours a current of 166 µA is measured, which is negligible compared to the current just after removing the light source (9.585 mA / 9585 µA). In the time between 20 hours and 62 hours of discharge, the current still decreased to a value of 81.423 µA, but since the current after 20 hours is significantly low, it can be said that the cell is discharged after 20 hours of resting in the dark. The same analysis can be made for the blue curve, which shows that after 29 hours and 18 minutes a current of 166 µA is measured. This value is also compared to the last measured value, after 48 hours. During this period the current still decreased to a value of 97.0 µA. When compared to the current just after removing the light source (12.5 mA / 12508.6 µA), the 2 above values can be neglected and the conclusion can be made that the cell is discharged after 29 hours and 18 minutes.

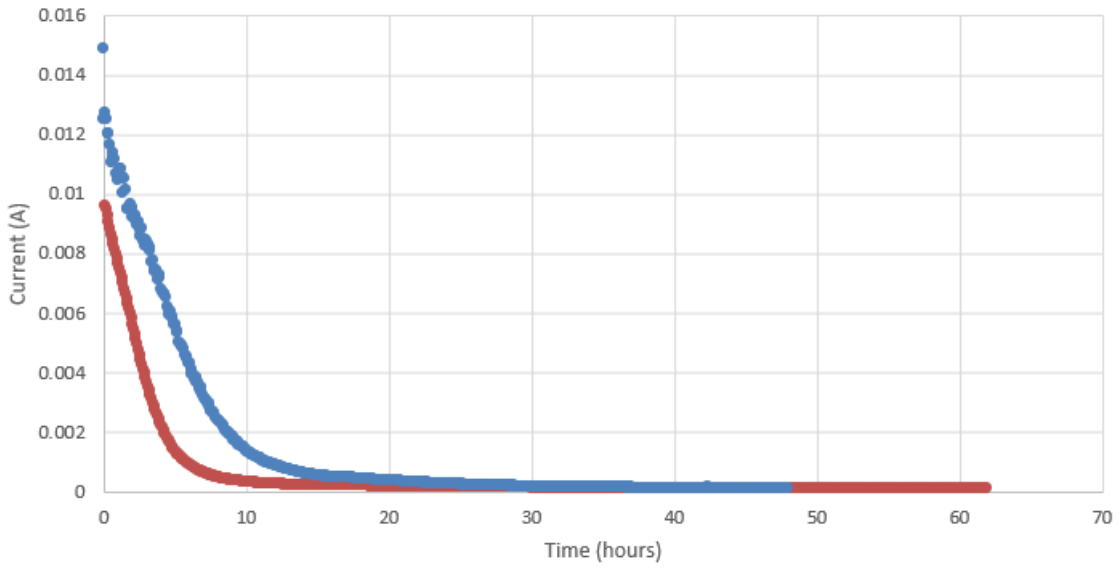

Figure 23: (Red) CIGS 5%-O dark measurement at 700 mV after 15 minutes of light illumination – (Blue) CIGS 5%-O dark measurement at 700 mV after 90 minutes of light illumination

The CZTS cell with an i-ZnO layer having an oxygen content of 5% was also exposed to sunlight at an intensity of 86.6 mW/cm² for 90 minutes and then placed in the dark. The discharge process is visible in Figure 24a. For this cell, a bias voltage of 500 mV was applied. As visible in Figure 24a, the cell discharges very quickly compared to the CIGS cells. A possible reason for this faster discharge is the use of a lower bias voltage. Between 3.5 hours and 14.5 hours a constant current of 17.6 µA is reached. After 14.5 hours, a dropdown in the curve occurs. From this dropdown until the end of the measurements, the current increases slightly over a period of 26 hours. Without changing the setup,

an IV curve was preformed after this test of 42 hours and is shown in Figure 24a. This figure shows that the cell is broken. This is a possible explanation of the drop down visible in Figure 24b. Hence, it appears that our CZTS devices breakdown after a certain amount of time making it difficult to further investigate this class of devices. While the i-ZnO layer is likely related to the synaptic behavior, the CZTS absorber does not support a constant 0.5V bias over several hours; the reasons for this junction breakdown are unclear for now and could be an anomaly of this batch of solar cells. This result will need confirmation with another series of samples.

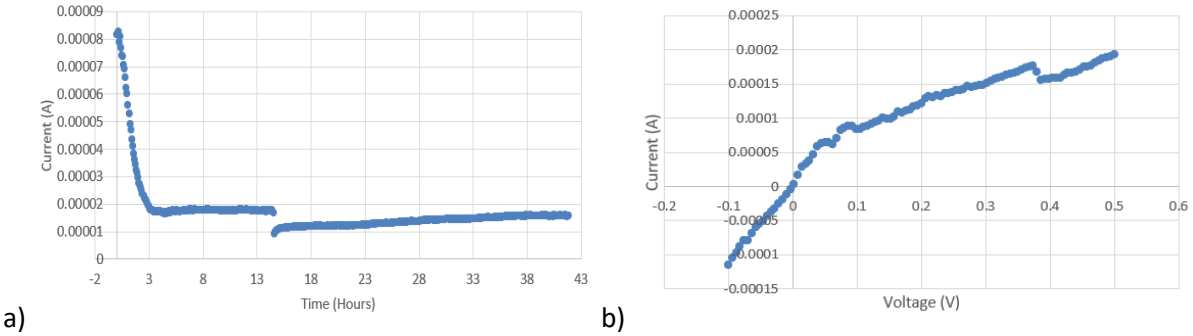

a) b)

Figure 24: a) CZTS 5%-O dark measurement at 500 mV after 90 minutes of light illumination b) The IV-curve after the dark measurement

3.2 The influence of different wavelengths

Because different CZTS cells broke down during the first tests, there is no possibility to continue testing with the CZTS cells. As a result, the influence of different wavelengths is only tested with the CIGS cells. To begin, the CIGS 5%-O cell is irradiated with sunlight for 15 minutes at an intensity of 86,6 mW/cm². Then, all wavelengths are set to an intensity of 0 mW/cm² and are activated one by one with an intensity of 1,4 mW/cm². For each wavelength, a measurement starts for 80 seconds with a specific bias voltage of 0 mV (I_{SC}). During the test time, the light source is switched on and off every 10 seconds. As a result, we obtain the result shown in Figure 25.

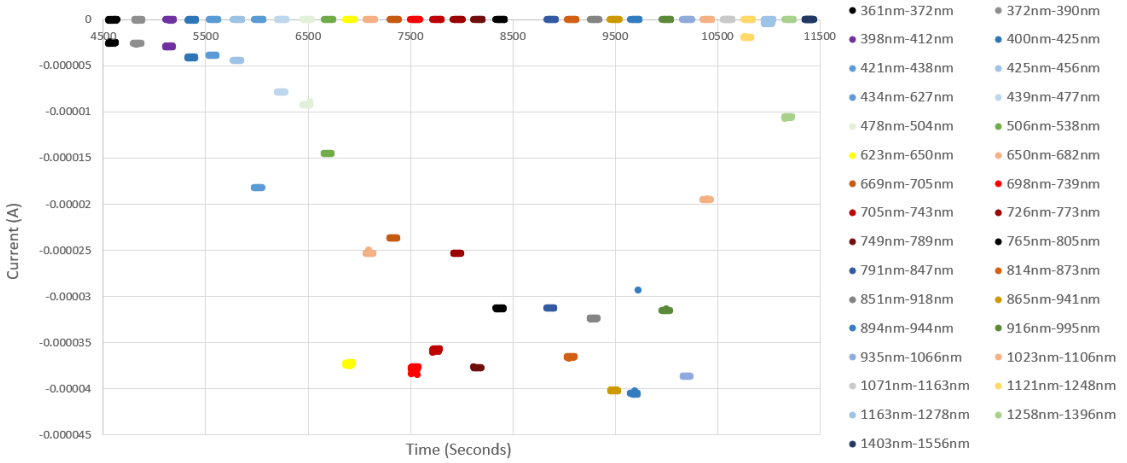

Figure 25: The effect of different wavelengths at an intensity of 1,4 mW/cm² at a bias voltage of 0 mV (I_{SC}) at the CIGS 5%-O cell

Figure 25 shows that at a bias voltage of 0 mV, the cell behaves like a sensor rather than a memory. The cell reacts when the light source is turned on, but no memory effect occurs. There is an abrupt transition from when the light source is active to when the light source is inactive. Certain wavelengths affect the cell to a significantly greater extent than other wavelengths. Wavelengths 894 nm - 944 nm, as shown in Figure 26b, have the most impact on the cell, with a current difference between on and

off of 40.5 µA. This is significantly greater than the current difference at the smallest wavelength (361 nm - 372 nm), as shown in Figure 26a, which is equal to 2.5 µA.

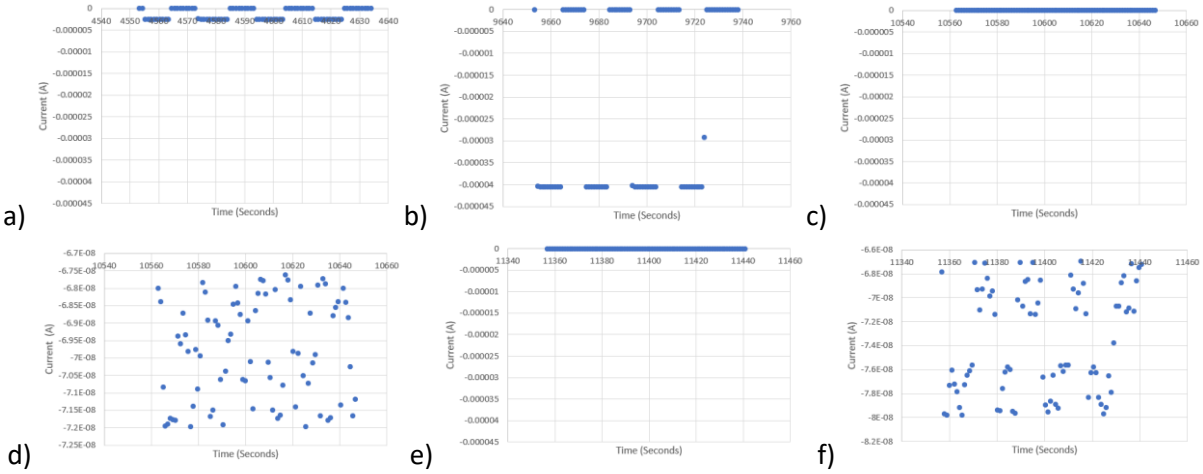

Figure 26: a) The effect of wavelengths 361 nm – 372 nm at 0 mV (I_{SC}) at the CIGS 5%-O cell b) The effect of wavelengths 894 nm – 944 nm at 0 mV (I_{SC}) at the CIGS 5%-O cell c) The effect of wavelengths 1071 nm – 1163 nm at 0 mV (I_{SC}) at the CIGS 5%-O cell d) Zoomed at wavelengths 1071 nm – 1163 nm e) The effect of wavelengths 1403 nm – 1556 nm at 0 mV (I_{SC}) at the CIGS 5%-O cell f) Zoomed at wavelengths 1403 nm – 1556 nm

Figure 25 also shows two wavelengths which do not have an impact, these are the wavelength 1071 nm - 1163 nm, shown in Figure 26c and the wavelengths 1403 nm - 1556 nm, shown in Figure 26e. When zooming in on the result of the wavelengths 1071 nm - 1163 nm, the effect of these wavelengths becomes clearer and is shown in Figure 26d. It is clearly shown that the current varies randomly in a range of 4.5 nA and there is no possibility of obtaining a digital signal from these wavelengths as with the other wavelengths. Also at the wavelengths 1403 nm - 1556 nm (IR), we focus to investigate the impact and in contrast to the wavelengths 1071 nm - 1163nm, a partition is present here. Except for one point, there is no measurement point between -72 nA and -76 nA. Of course, these are very small currents, but still these wavelengths have a small impact on the cell.

The above tests are repeated under the same conditions, only the bias voltage is increased from 0 mV to 700 mV. The result is shown in Figure 27. Compared to the result at a bias voltage of 0 mV, there is no longer a clear on-off situation visible. To discuss the impact of the different wavelengths, we need to zoom in on each wavelength.

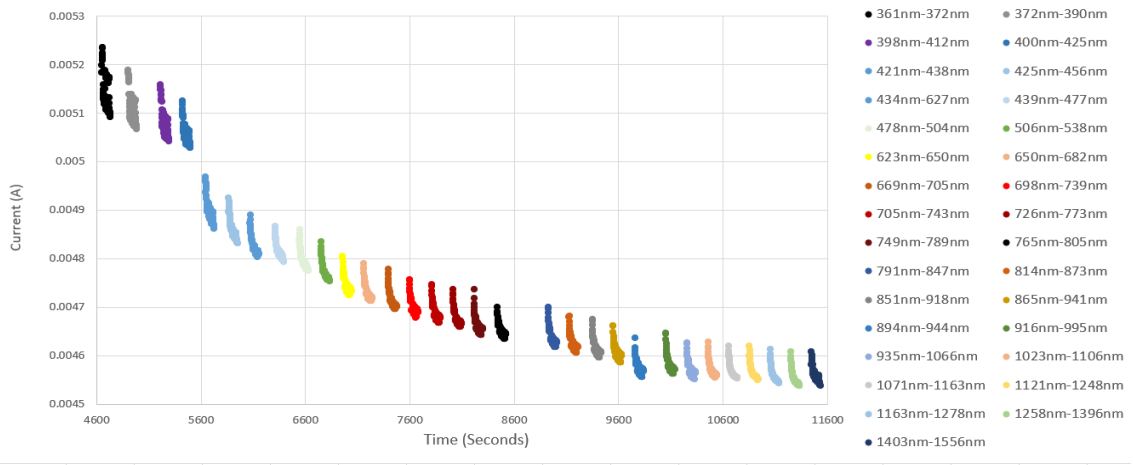

Figure 27: The effect of different wavelengths at an intensity of 1,4 mW/cm² at a bias voltage of 700 mV at the CIGS 5%-O cell

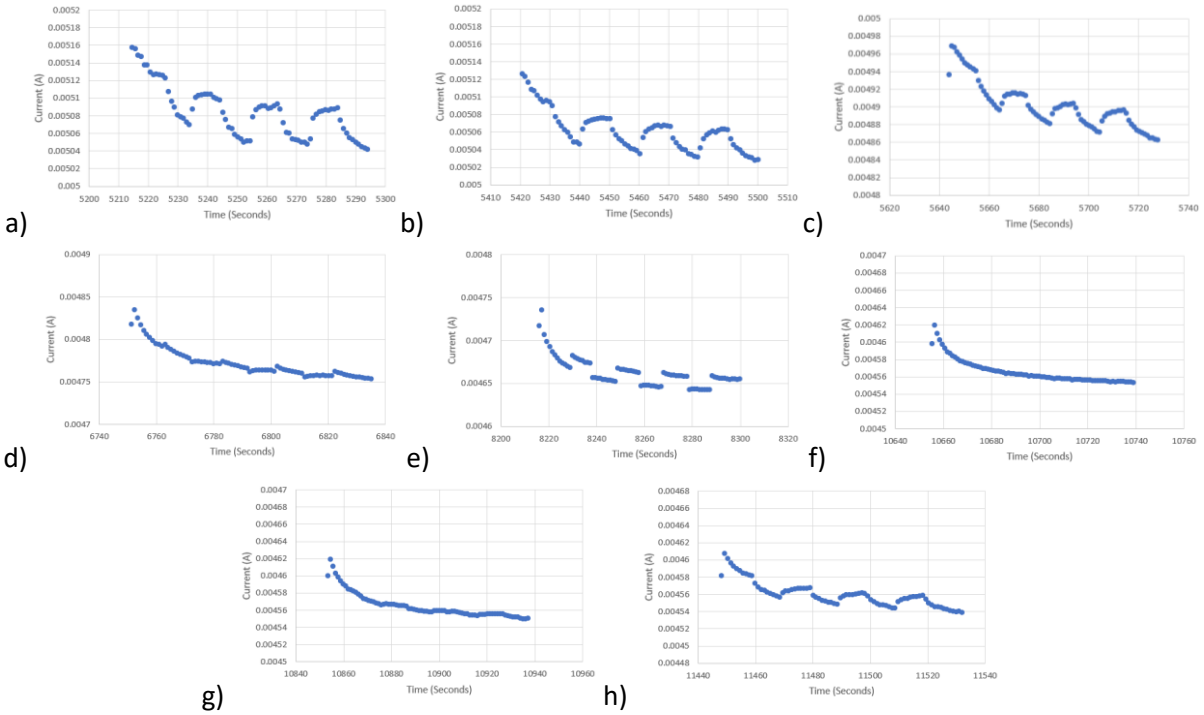

Figure 28: a) The effect of wavelengths 398 nm – 412 nm at 700 mV at the CIGS 5%-O cell b) The effect of wavelengths 400 nm – 425 nm at 700 mV at the CIGS 5%-O cell c) The effect of wavelengths 421 nm – 438 nm at 700 mV at the CIGS 5%-O cell d) The effect of wavelengths 506 nm – 538 nm at 700 mV at the CIGS 5%-O cell e) The effect of wavelengths 749 nm – 789 nm at 700 mV at the CIGS 5%-O cell f) The effect of wavelengths 1071 nm – 1163 nm at 700 mV at the CIGS 5%-O cell g) The effect of wavelengths 1121 nm – 1248 nm at 700 mV at the CIGS 5%-O cell h) The effect of wavelengths 1403 nm – 1556 nm at 700 mV at the CIGS 5%-O cell

Given the chosen current convention, a current increasing from illumination will be attributed to photoconductivity of the system, while a current decreasing is photocurrent generated in the absorber.

Figure 28d shows the first wavelengths (506 nm - 538 nm) where little to no synaptic response is visible. The wavelengths 749 nm - 789 nm, visible in Figure 28e, have the largest current difference between the on and off state, which corresponds to a photocurrent generated in the absorber, but no memory effect is visible indicating that the level responsible for the persistent photoconductivity is not activate at this energy.. This effect occurs until and including the wavelengths 1023nm - 1106 nm, all of which are well absorbed by the CIGS absorber. The wavelengths smaller than 506 nm - 538 nm have no on-off state, but have a continuous curve, as visible in Figure 28a, Figure 28b and Figure 28c. These curves show a transition between the on and off state, a very important property for creating an analog memory as illustrated Figure 29. The behavior shown at these wavelengths corresponds to the behavior of an RC circuit integrator. It should be especially highlighted that such behavior is also observed in Figure h, at a wavelength where light does not interact with the absorber; similarly, a strong synaptic plasticity is observed for high energy photons, which are in their very large majority absorbed by the ITO/i-ZnO window layer rather than the absorber ; hence, the level(s) responsible for the memory effect are in all likelihood located in the ZnO layer, and can possibly be tuned by adjusting the oxygen content. In an RC integrator, when an input voltage is applied (stimulus), the output voltage will gradually increase. From the moment the input voltage disappears, the output voltage will fall back gradually as seen in Figure 29. The resulting figure of merit has a similar shape as that of our solar cell under specific wavelengths, which thus behaves as wavelength depending sensing and a memory unit.

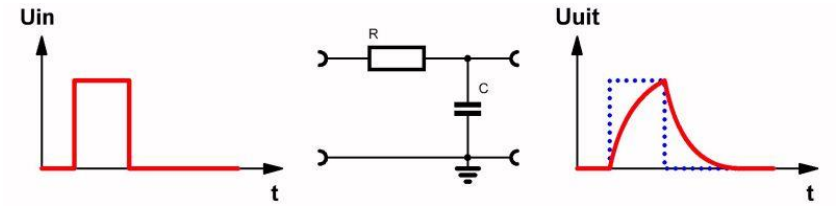

Figure 29: RC circuit integrator[19]

It is particularly important to focus on Figure 28f, Figure 28g and Figure 28h. While no memory effect is observed for the first two, The RC circuit behavior is again visible at the wavelengths 1403 nm - 1556 nm, which is well below the absorption threshold of the CIGSe and thus does not generate any photocurrent.

In the next part, this wavelength is investigated as a probe to the system investigating if the synaptic behavior at such wavelength depends on the initial state of the system (potentiated or depressed). First, the cell is irradiated for a certain time with sunlight. After this, a test starts for 80 seconds at a bias voltage of 700 mV, turning the light source on or off every 10 seconds. The light source is set to the wavelengths 1403 nm - 1556 nm with an intensity of 1.4 mW/cm². Figure 30a shows this result, with a clear potentiation depression cycle. This test is repeated but with a fully depressed cell, Figure 30b showing this result. In the latter case, absolutely no response is obtained. This result is one of the major observation of this work; not only is the system wavelength sensitive, offering variable programming states as a function of the wavelength, but a specific IR wavelength allows to probe the state of the system. While uncertain at this point, such behavior tends to indicate that more than one sub-gap intermediate state is involved in the process.

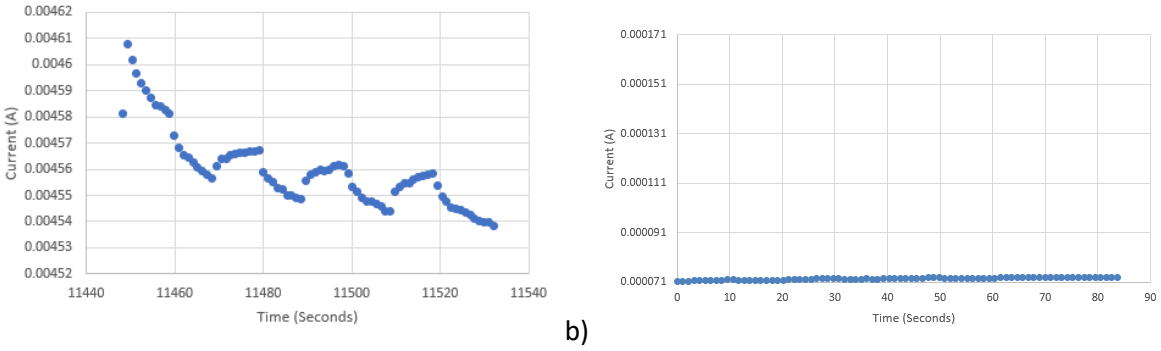

Figure 30: a) The effect of wavelengths 1403 nm – 1556 nm at 700 mV at a charged cell b) The effect of wavelengths 1403 nm – 1556 nm at 700 mV at a discharged cell

Based on these results, two methods can be used to identify the difference between a charged and a discharged cell. The first method looks at the measured current. For the discharged cell the current is constant and equal to 72.5 µA, while the average measured current for this charged cell is equal to 4.56 mA. The conclusion is that as long as the current is greater than about 72.5 µA the cell is not fully discharged. The second method looks at the current difference between the moment just before the light source is turned on and just before the light source is turned off. For a discharged cell this difference is equal to 0, while for the charged cell the difference is equal to 10.7 µA.

3.3 The influence of the oxygen content

The same test procedure was then repeated for the CIGS 15%-O cell. Again, the effect of different wavelengths at a bias voltage of 0 mV (I_{SC}) was tested and results in the same behavior as the CIGS 5%-O cell, the only difference is the value of the short circuit current, these is twice de value of the

short circuit current of the CIGS 5%-O. This is in contrast to the result at a bias voltage of 700 mV where the result is different for each wavelength compared to the CIGS 5%-O cell. Figure 31 shows the results of the effect of the different wavelengths at 700 mV at the CIGS 15%-O cell.

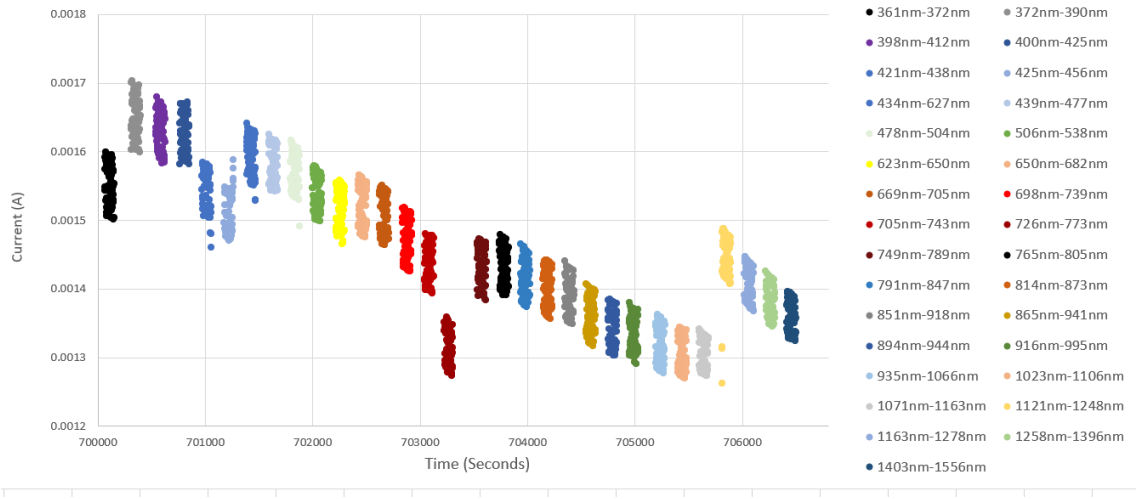

Figure 31: The effect of different wavelengths at an intensity of 1,4 mW/cm² at a bias voltage of 700 mV at the CIGS 15%-O cell

Again, the light source was switched on and off every 10 seconds, but a memory effect is not visible at all. Figure 32a, Figure 32b and Figure 32c shows the result of 3 different ranges of wavelengths. The scale at which these are plotted corresponds to the scale of Figure 28. It is visible that the measuring points are all around and that there is no structure present and therefore also no memory effect.

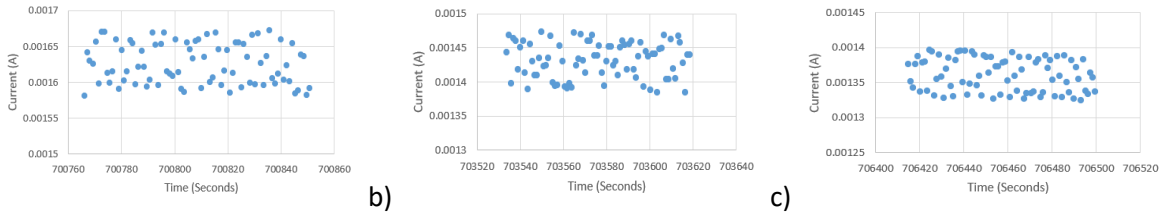

Figure 32: a) The effect of wavelengths 400 nm – 425 nm at 700 mV at the CIGS 15%-O cell b) The effect of wavelengths 749 nm – 789 nm at 700 mV at the CIGS 15%-O cell c) The effect of wavelengths 1403 nm – 1556 nm at 700 mV at the CIGS 15%-O cell

Also with the CIGS 0%-O cell, these tests were performed at a bias voltage of 0 mV and a bias voltage of 700 mV. The results at 0 mV are again the same as for the two previous CIGS cells, the only difference is the value of the short circuit current, which is twice the value of the short circuit current of the CIGS 5%-O. No memory effect was obtained at low wavelengths at a bias voltage of 700 mV, as shown in Figure 33a and Figure 33b. These figures show that the light source has no effect at these wavelengths, there is no difference between light illumination and no light illumination. From the wavelengths 749 nm - 941 nm up to the wavelengths 1023 nm - 1106 nm, an imperfect analog memory effect is obtained with slightly erratic data, as seen in Figure 33c and Figure 33d. As also observed for the CIGS 5%-O, there is absolutely no effect at the wavelengths 1071 nm - 1163 nm, as shown in Figure 33e. For the wavelengths larger than 1071 nm - 1163nm, the curve becomes increasingly better and more similar as the curve of the RC integrator. For IR light, the best result is obtained as visible in Figure 33g.

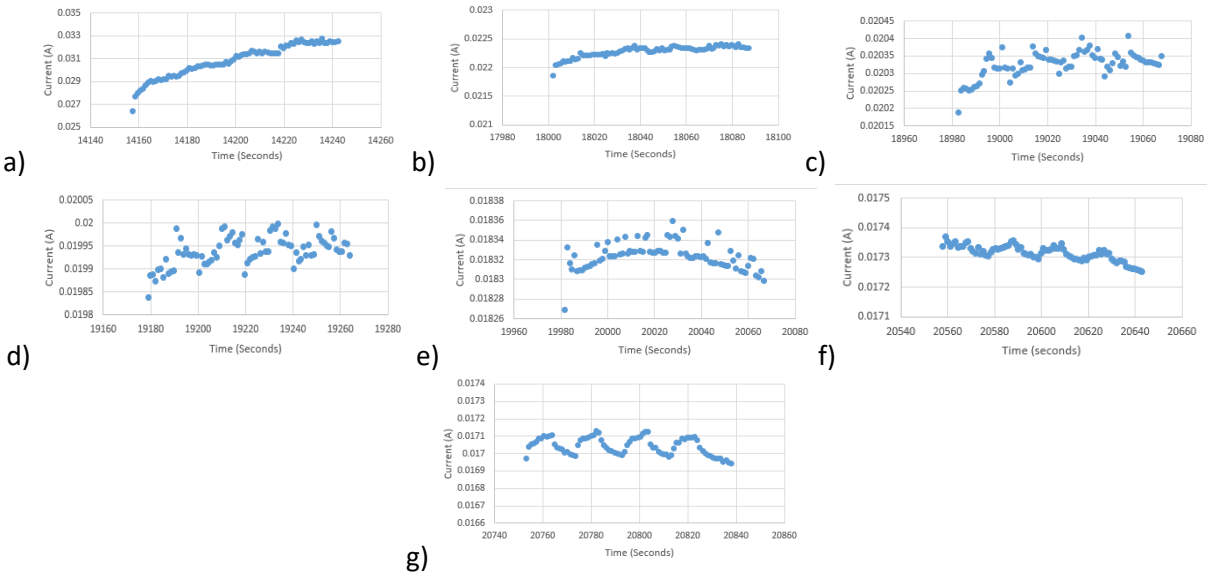

Figure 33: a) The effect of wavelengths 400 nm – 425 nm at 700 mV at the CIGS 0%-O cell b) The effect of wavelengths 749 nm – 789 nm at 700 mV at the CIGS 0%-O cell c) The effect of wavelengths 865 nm – 941 nm at 700 mV at the CIGS 0%-O cell d) The effect of wavelengths 894 nm – 944 nm at 700 mV at the CIGS 0%-O cell e) The effect of wavelengths 1071 nm – 1163 nm at 700 mV at the CIGS 0%-O cell f) The effect of wavelengths 1258 nm – 1396 nm at 700 mV at the CIGS 0%-O cell g) The effect of wavelengths 1403 nm – 1556 nm at 700 mV at the CIGS 0%-O cell

Finally, the above tests are also performed on the CIGS 10%-O cell. At and bias voltage of 0 mV (I_{SC}), the same result was obtained as with each test. Also the value of I_{SC} corresponds to the value of the CIGS 5%-O cell. Also for the CIGS 10%-O cell at a bias voltage of 700 mV, a memory effect is observed. The memory effect is less clearly present compared to the CIGS 5%-O cell. The memory effect also occurs only at the first 4 ranges of wavelengths, as visible in Figure 34a, Figure 34b, Figure 34c and Figure 34d.

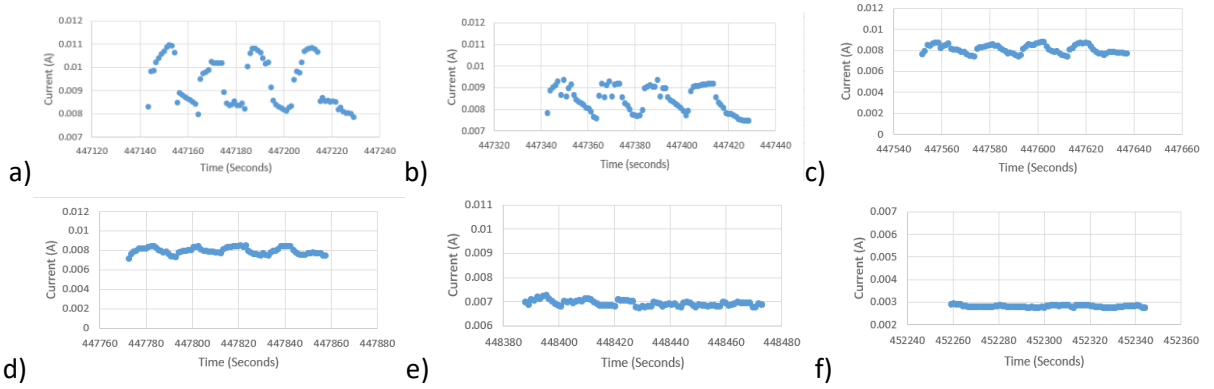

Figure 34: a) The effect of wavelengths 361 nm – 372 nm at 700 mV at the CIGS 10%-O cell b) The effect of wavelengths 372 nm – 390 nm at 700 mV at the CIGS 10%-O cell c) The effect of wavelengths 398 nm – 412 nm at 700 mV at the CIGS 10%-O cell d) The effect of wavelengths 400 nm – 425 nm at 700 mV at the CIGS 10%-O cell e) The effect of wavelengths 434 nm – 627 nm at 700 mV at the CIGS 10%-O cell f) The effect of wavelengths 1023 nm – 1106 nm at 700 mV at the CIGS 10%-O cell

At larger wavelengths, there is no memory effect visible at all. The curves are not completely flat, but no clear behavior is visible between the on and off state and vice versa, the wavelengths 434 nm - 627 nm and wavelengths 1023 nm - 1106 are shown in Figure 34e and Figure 34f. As a result, it is concluded that these wavelengths are not useful as a memory element.

After investigating the CIGS cells with different oxygen content, the conclusion can be made that the optimal oxygen content in ZnO for obtaining the desired memory effect corresponds to 0% and 5%.

Depending on the used wavelengths, a particular CIGS cell will be chosen. For CIGS 5%-O cell, low wavelengths will be used to get the desired result, while for the CIGS 0%-O cell, the large wavelengths will provide the best memory effect.

3.4 Stimulated depression of the synapse from IR illumination

As mentioned earlier, the CIGS 5%-O cell is discharged when the current at a bias voltage of 700 mV is equal to or less than 166 µA. At a light illumination time of 15 minutes, the cell takes 20 hours to discharge. Next, a discharged cell was irradiated with sunlight (86.6 mW/cm²) again for 15 minutes. After this the cell was irradiated again for 15 minutes but now with IR light (1403 nm - 1556 nm) with an intensity of 1.4 mW/cm², this because IR is not absorbed by the CIGSe and doesn't generate photocurrent. Figure 35a shows the 2 different discharge curves. The green curve shows the discharge after sunlight only and the green curve is the discharge after sunlight and IR. The red curve is steeper than the green curve and thus discharges faster, which indicates that the extra step of IR illumination has stimulated the discharge. This observation is consistent with the previously discussed hypothesis that not one but two intermediate levels are involved; indeed, the IR light possibly promotes trapped carriers from a deep, long lifetime state, to a slightly less deep and shorter lifetime state, thus promoting a faster discharge of the system. The red curve reaches its discharged state after 8 hours and 45 minutes. With IR light, the cell discharges 11 hours and 15 minutes faster than under normal conditions.

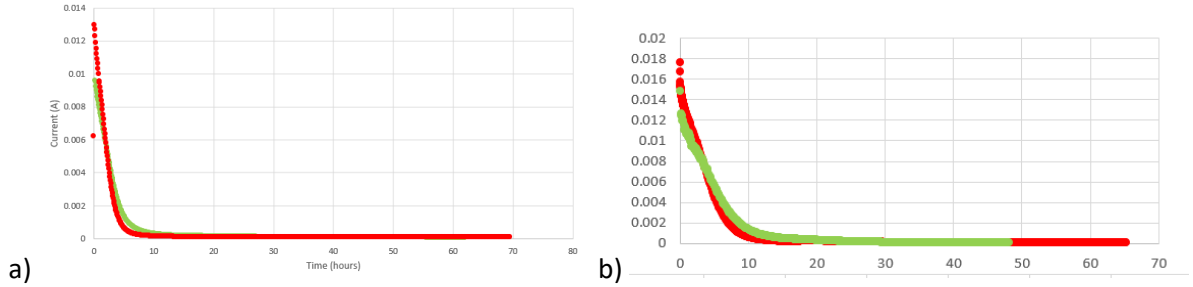

Figure 35: a) (Green) CIGS 5%-O dark measurement at 700 mV after 15 minutes of light illumination (sunlight) - (Red) CIGS 5%-O dark measurement at 700 mV after 15 minutes of light illumination (sunlight) and 15 minutes of light illumination with the wavelength of 1403 nm – 1556 nm b) (Green) CIGS 5%-O dark measurement at 700 mV after 90 minutes of light illumination (sunlight) - (Red) CIGS 5%-O dark measurement at 700 mV after 90 minutes of light illumination (sunlight) and 90 minutes of light illumination with the wavelength of 1403 nm – 1556 nm

As previously mentioned, a cell with an illumination time of 90 minutes takes 29 hours and 18 minutes to discharge. Then the same discharged cell was irradiated with sunlight (86.6 mW/cm²) for 90 minutes and after this it was irradiated again, but now with IR light (1403 nm - 1556 nm) for 90 minutes. Figure 34b shows the result. The red curve is the discharge process with only sunlight and the blue curve is the discharge process with sunlight and IR light. The discharge curve of sunlight and IR light is again steeper than the other curve, so the cell discharges faster after exposure to IR light. The blue curve takes 22 hours and 24 minutes to reach a current of 166 µA, from this point is the cell discharged. This is 6 hours and 54 minutes faster than the discharge process after only sunlight. The effect of IR light accelerating the synaptic depression is thus reproducible with different illumination duration, and thus different injections of charge carriers to the trap level.

3.5 The change of I_{SC} under light illumination

Tests were performed only on the CIGS 5%-O cell, to try to observe a memory effect in short circuit conditions similar to what has previously been reported in DSSC[14]. Figure 36 shows the current at a bias voltage of 0 mV (I_{SC}) under light illumination for the CIGS cells 5%. These measurements were

always performed at a discharged cell. The blue curve is the first test, which shows that after 1260 seconds the current stabilizes with a value of -1.1712 mA. Then a few days later a second test was performed (red) and this showed a stabilization after 800 seconds at a current of -1.1642 mA. So there is a difference of 7.2 µA between the first and the second test and also the stabilization time is different. Furthermore, a third test was performed (purple) which is closer to the result of the first test. In this test the current stabilizes after 1500 seconds at a value of -1.1688 mA. the current difference with the first test is equal to 2.4 µA. The behavior before stabilizing is similar with the charge phase of the RC integrator, but there no similar discharge phase. To conclude if the short circuit current under light illumination can be used as an analog memory, more investigation is needed.

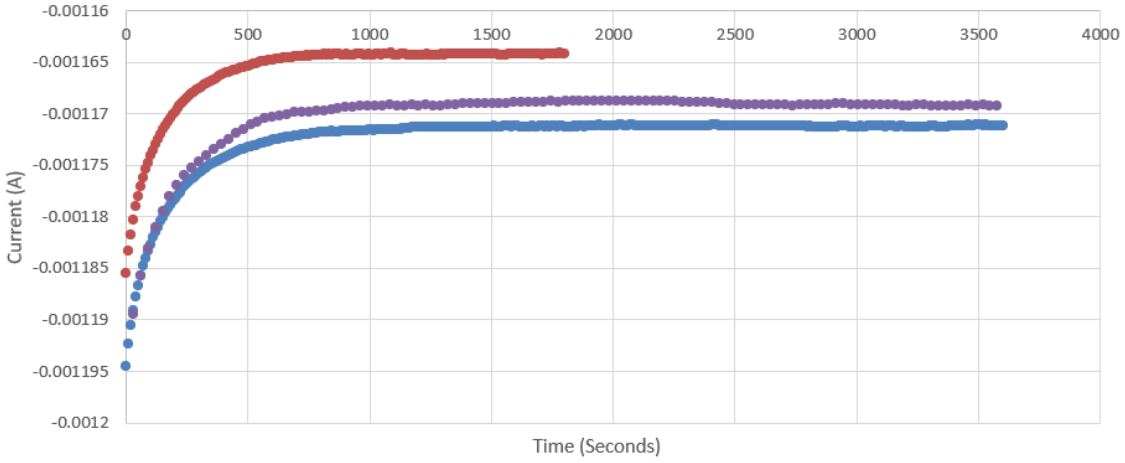

Figure 36: (Blue) CIGS 5%-O light illumination measurement at 0 mV (I_{SC}) first time – (Red) CIGS 5%-O light illumination measurement at 0 mV (I_{SC}) second time - (Purple) CIGS 5%-O light illumination measurement at 0 mV (I_{SC}) third time

4. Conclusion

In this work, we demonstrated unequivocally that CIGSe solar cells can function as artificial synapses with a clear plasticity observed, and ascribed to oxygen related long lifetime traps present in the i-ZnO window layer. Various oxygen contents where investigated in that context. When there is too much oxygen content (CIGS 15%-O) no analog memory effect is detected at all. The most obvious and useful analog memory effect is present with the CIGS 0%-O and CIGS 5%-O cell (optimum in our experiments), though the physical details on the trap density and transition energies involved remain to be carefully investigated. Importantly, the analog memory effect was detected with variations for different wavelengths, which implies an energy selectivity in the synaptic response of the system and allows for more programming states than if the system was functioning with electrical stimuli.

A consequence of this wavelength selectivity is the possibility to probe whether a cell is charged or discharged using IR illumination below the absorber's bandgap. If the cell is discharged no impact will be noticeable. In addition to determining whether a cell is charged or discharged, IR light can also accelerate the discharge process of a charged cell. If the cell is discharged, the IR illumination has no impact on the system. If the system is charged in its initial state, the system will exhibit a potentiation/depression cycle upon IR illumination, which hints at the possibility of a system with more than one sub-gap intermediate state. In addition to determining whether a cell is charged or discharged, IR light can also accelerate the discharge process (depression) of a charged cell. If a charged cell is exposed to IR light for a certain duration and then placed in the dark, the discharge process will be quicker. Furthermore, the illumination time also has an influence on the discharge time. The longer the cell is irradiated, the longer the cell takes to discharge, though the depression effect of IR light remains consistently observed.

Furthermore, a memory effect is also detected at a bias voltage of 0 mV (Isc) during light illumination, reproducing well past results obtained on DSSC. After a certain time, the current stabilizes each time, but always at a different value. Further research is needed to explain this behavior better, as both photocurrent and persistent photoconductivity due to trap states in the i-ZnO interplay.

In the current state of this work, the exact physical phenomena and metastabilities involved in the synaptic plasticity are yet to be fully understood and this report paves the way to further investigations. It is suspected that the existence of oxygen related trap states in the i-ZnO layer lead to the observed persistent photoconductivity, which opens the possibility of devices functioning without a PV absorber, and for example making use of a Schottky diode instead; this would allow to suppress the possible screening of the synaptic behavior by the unwanted photocurrent at intermediate wavelengths.

References

[1] 'Kunstmatige intelligentie en machine learning: hype of toekomstbestendig bedrijfsmodel', *Emerce*. https://www.emerce.nl/achtergrond/kunstmatige-intelligentie-en-machine-learning-hype-of-toekomstbestendig-bedrijfsmodel (accessed Apr. 19, 2022).

[2] H.-X. Wang, R. C. Gerkin, D. W. Nauen, and G.-Q. Bi, 'Coactivation and timing-dependent integration of synaptic potentiation and depression', *NATURE NEUROSCIENCE*, vol. 8, no. 2, p. 7, 2005.

[3] L. A. Santschi and P. K. Stanton, 'A paired-pulse facilitation analysis of long-term synaptic depression at excitatory synapses in rat hippocampal CA1 and CA3 regions', *Brain Research*, p. 15, 2003.

[4] B. Widrow, Y. Kim, D. Park, and J. K. Perin, 'Nature's Learning Rule', in *Artificial Intelligence in the Age of Neural Networks and Brain Computing*, Elsevier, 2019, pp. 1–30. doi: 10.1016/B978-0-12-815480-9.00001-3.

[5] A. Huang, X. Zhang, R. Li, and Y. Chi, 'Memristor Neural Network Design', in *Memristor and Memristive Neural Networks*, A. P. James, Ed. InTech, 2018. doi: 10.5772/intechopen.69929.

[6] F. Rosenblatt, 'The perceptron: A probabilistic model for information storage and organization in the brain.', *Psychological Review*, vol. 65, no. 6, pp. 386–408, 1958, doi: 10.1037/h0042519.

[7] S. Cohen, 'The basics of machine learning: strategies and techniques', in *Artificial Intelligence and Deep Learning in Pathology*, Elsevier, 2021, pp. 13–40. doi: 10.1016/B978-0-323-67538-3.00002-6.

[8] D. Krotov and J. J. Hopfield, 'Unsupervised learning by competing hidden units', *Proc. Natl. Acad. Sci. U.S.A.*, vol. 116, no. 16, pp. 7723–7731, Apr. 2019, doi: 10.1073/pnas.1820458116.

[9] S. Mirjalili, J. Song Dong, and A. Lewis, Eds., *Nature-Inspired Optimizers: Theories, Literature Reviews and Applications*, vol. 811. Cham: Springer International Publishing, 2020. doi: 10.1007/978-3-030-12127-3.

[10] M. Boden, 'A guide to recurrent neural networks and backpropagation', p. 10.

[11] *Neural Circuit Development and Function in the Brain*. Elsevier, 2013. doi: 10.1016/C2011-0-07732-3.

[12] L. H. *et al.*, 'A learnable parallel processing architecture towards unity of memory and computing', *Scientific Reports*, p. 9.

[13] Y.-G. Bao and S. Wang, 'Labeled von Neumann Architecture for Software-Defined Cloud', *J. Comput. Sci. Technol.*, vol. 32, no. 2, pp. 219–223, Mar. 2017, doi: 10.1007/s11390-017-1716-0.

[14] H. N. Tsao and M. Grätzel, 'Illumination Time Dependent Learning in Dye Sensitized Solar Cells', *ACS Appl. Mater. Interfaces*, vol. 10, no. 43, pp. 36602–36607, Oct. 2018, doi: 10.1021/acsami.8b12027.

[15] S. M. Sze and K. K. Ng, *Physics of semiconductor devices*, 3. ed. Hoboken, NJ: Wiley-Interscience, 2007.

[16] 'Theory of solar cells', *Wikipedia*. Nov. 07, 2021. Accessed: Apr. 18, 2022. [Online]. Available: https://en.wikipedia.org/w/index.php?title=Theory_of_solar_cells&oldid=1054006486

[17] A. Marti and A. Luque, 'Electrochemical Potentials (Quasi-Fermi Levels) and the Operation of Hot-Carrier, Impact-Ionization, and Intermediate-Band Solar Cells', *IEEE J. Photovoltaics*, vol. 3, no. 4, pp. 1298–1304, Oct. 2013, doi: 10.1109/JPHOTOV.2013.2274381.

[18] 'Electrometers'. https://www.tek.com/en/products/keithley/low-level-sensitive-and-specialty-instruments/electrometers (accessed May 03, 2022).

[19] 'Elektronica-hobby blog van Jos Verstraten (525 artikelen): Theorie-13: RC-kringen', *Elektronica-hobby blog van Jos Verstraten (525 artikelen)*. https://verstraten-elektronica.blogspot.com/p/rc-kringen.html (accessed May 17, 2022).